



CHARACTERIZING ADDITIVE MANUFACTURING: PRECIPITATION HARDENING STAINLESS STEEL (15-5 PH)

Alex M. da S. Costa¹, Claudio T. dos Santos¹, Cristiane E. R. Silva¹,
Edwin Sallica-Leva¹, Maurício J. Monteiro¹, Nilton Vieira Larcher^{1*},
Sheyla Santana de Carvalho¹, Wellington G. Fernandes¹

1 - Instituto Nacional de Tecnologia (INT/MCTI) – Divisão de Materiais (DIMAT)- Laboratório de
Caracterização Microestrutural e de Propriedades Mecânicas (LACPM).
Av. Venezuela, 82 – Saúde – Rio de Janeiro, CEP 20081-312, RJ.
nilton.vieira@int.gov.br

ABSTRACT

Owing to many technological improvements on related areas, additive manufacturing has turning into an important way to produce costumized parts with unique shapes and properties for a range of applications, although there are yet many challenges ahead for improvements and fine tuning. In this context, a traditionally material used by the aircraft industry, a precipitation hardening stainless steel, 15-5 PH, built by laser-powder bed fusion, is characterized in the present work. Metallic powder, as-built and as solution treated samples were characterized. The characterization of the metallic powder presented: thin volume fraction ($<1 \mu\text{m}$) was under 1% and particle average size was $42 \mu\text{m}$, both results were obtained by laser diffraction; density of 7.76 g/cm^3 , obtained by Helium pycnometer; and retained austenite fraction of 1.71 %, in a matrix of martensite, was obtained by X-ray diffraction using Bragg-Brettano geometry, after Rietveld refining method on the powder pattern. The characterization of the as-built part, porosity was evaluated of 1.7%. The predominantly martensitic microstructure evolved its morphology from very refined, in the as-built condition, to less refined, in the as solution treated condition. The as-built sample was also analyzed: in electron scanning-transmission microscopy by focused ion beam (FIB-STEM), which revealed high dislocation density and precipitates; in X-ray diffraction, under the previously mentioned conditions, where the retained austenite obtained was 2.63%; in mechanical testing, whose mechanical properties measured were 202 GPa of Young Modulus, 814 MPa of yield strength, 1,243 MPa of ultimate tensile strength and 18% of elongation. Subsequent to the tensile testing, the fracture surface of the specimen was evaluated in scanning electron microscopy (SEM), which revealed ductile features owing to the presence of high number of dimples.

Keywords: *Precipitation-hardening stainless steel, 15-5 PH, Additive Manufacturing Characterization, Microstructure, Mechanical properties.*

INTRODUCTION

Additive manufacture (AM) has been intensively explored and used with several different purposes ⁽¹⁾. In this context, a material used by the aircraft industry, a precipitation hardening (PH) stainless steel was built by laser-powder bed fusion (L-PBF).

AM process is very different from the traditional ones and, in many cases we are still learning the best configuration set to meet our expectations and needs. That is exactly where and when characterization takes a major role in the process.

15-5 PH steel is a very complex material ^(2,3), an iron-based alloy with Cr, Ni, Cu, Nb, very low C content along with other small weight fraction elements. Precipitation is the main

hardening mechanisms (HM) operating ⁽⁴⁾. Nanometric copper precipitates homogeneously distributed throughout the matrix harden the steel, owing to the coherent interface with the matrix. Martensitic transformation ⁽⁵⁾ is another important HM, since martensite (α' phase (bcc)) is the major microstructural component, along with AM thermal cycles are responsible for creating high density of dislocations that accommodates deformations ⁽⁶⁾, which is another HM. The second major component is retained austenite (γ phase (fcc)). Other precipitates are present such as NbC, possibly, Cr₃C₂, and multielemental ones (G-phase) among others, depending on the chemistry ⁽⁷⁾. These are always challenging to detect and identify. Advanced techniques should be effective, such as small angle X-rays scattering (SAXS⁽⁷⁾), high-energy X-rays diffraction (HEXRD)⁽⁸⁾, electron backscattered diffraction (EBSD) ⁽⁷⁾, transmission electron microscopy (TEM) ⁽⁵⁾ and/or atom probing tomography (APT) ⁽⁹⁾.

In L-PBF, the interaction between laser (quality, power, diameter, scanning speed, hatching distance and scanning strategy) and powder (particle size and distribution, particle shape, powder bed density, layer thickness and material properties) gives the part its features ^(1, 10, 11) and these are going to make it suitable for most applications.

MATERIALS AND METHODS

Material

EOS PH1 (15-5 PH Stainless Steel) powder was used for this study (Table 1).

Table 1: EOS PH1 powder chemistry (15-5 PH stainless steel grade): EOS Data Sheet and according to ASTM A564/A564M-13 standard (UNS S15500, type XM-12).

<i>Element</i>	Cr	Ni	Cu	Mn	Si	C	Mo	Nb	Fe
<i>Standard</i>	14.0 – 15.5	3.5 – 5.5	2.5 – 4.5	max 1.0	max 1.0	max 0.07	max 0.5	0.15 – 0.45	Balance
<i>EOS PHI</i>	14.0 – 15.5	3.5 – 5.5	2.5 – 4.5	max 1.0	max 1.0	max 0.07	max 0.5	0.15 – 0.45	Balance

Processing

An L-PBF ⁽¹⁾ process was employed was performed at PUC-Rio's Design Laboratory, where an EOS M-280 printer is located. An Yb fiber laser, in a N₂ plus 2% O₂ atmosphere, was employed aiming at random solid filling at 45°, with a 1.8 mm³/s volume rate building a 20 μ m thick layer. Three horizontal specimens, cylinder tensile testing like, were produced.

Methods

The metallic powder density was measured by gas Helium pycnometer (Ultrapycnometer 1000 by Quantachrome Instruments), at Laboratório de Tecnologia de Póis (LATEP), at INT. X-ray diffraction determined the crystallographic structure (diffractometer model D8 Advance by Bruker, at Laboratório de Aceleração em Processos Catalíticos (LACCA), at INT). A Bragg-Brentano geometry θ - 2θ was employed, scanning between 35 and 110° (with a 0.02° 2θ step), at room temperature, with copper radiation (wave length, $\lambda = 1.5418 \text{ \AA}$), the generator operated at 40 kV and 40 mA, with a nickel filter. Rietvelt refinement method was applied to the powder pattern, then the phase quantification analysis. Particle size distribution was obtaining by laser diffraction (CILAS 1064), at LATEP. The detectable sizes are from 0.04 μ m to 500 μ m. Additional morphological aspects were obtained by SEM (at CENANO/INT)/image analysis (Image J).

The as-built sample chemistry (Table 2) was analyzed by Spark Atomic Emission Spectrometry (ASTM E415-13/E415M-13 standard/ Oxford Instruments, model Foundry

Master Pro), at Universidade Federal de Santa Catarina's Laboratório de Engenharia Biomecânica (LEBm/UFSC). Hydrostatic weighing (Archimedes' principle) was employed to calculate the apparent density (scale by Shimadzu, model AUY220) at LATEP. X-ray diffraction, as mentioned before, was also used.

Table 2: 15-5 PH as-built chemistry.

<i>Element</i>	Cr	Ni	Cu	Mn	Si	C	Mo	Nb
<i>As-built</i>	14.6	4.35	3.49	0.127	0.521	0.0191	0.0951	0.297

As-built cross-section sample was prepared in a classic metallographic way. Villela's etchant was used. Optical Microscopy (OM) used a Olympus DP72, at Laboratório de Caracterização de Propriedades Mecânicas e Microestrutural (LACPM), at Divisão de Materiais (DIMAT), at INT. Scanning Electron Microscopy (SEM) with Energy Dispersive Spectroscopy (EDS) in a Field Emission Gun Scanning Electron Microscopy (Model QUANTA FEG 450, by FEI Company), at CENANO. Secondary (SE) and backscattered electrons (BSE) detectors were used. Focused Ion Beam/Scanning-Transmission Electron Microscope (Model HÉLIOS Nanolab DualBeam G3 CX, FEI Company), at CENANO, was also used.

Tensile testing was performed by an Instron static machine, model 3382, with 100 kN capacity, at LACPM. This test determined the Young Modulus (E), the Yield Strength (YS), and the Ultimate Strength (UTS), total elongation (El) and area reduction (AR) were calculated. Hardness testing was performed (ASTM-E92-17 standard) using a DigiTestor UH930 by Wolpert Wilson[®] Instruments, at LACPM. The Vickers' scale (HV 10) was used. The average of 10 measurements was considered the hardness value for the sample.

Solution treatment was performed in a muffle furnace by Quimis, 1045 °C (± 10 °C) for 45 min. and cooled down to room temperature, at LACPM.

RESULTS AND DISCUSSION

The average particle size distribution (Fig. 1) was 42.46 μm (SD = ± 0.9 μm). This result is within the range informed by L.F. Kultz Unti et al⁽³⁾ (15 – 45 μm , with 80% within this range), part of the distribution is on the thicker side (Fig 2a) and a small fraction ≤ 1 μm (0.4 %). SEM Image/Feret analysis enriched the results (Fig. 2b) with circularity (0.77 \pm 0.17) and aspect ratio (1.35 \pm 0.37). Some particles look like agglomerated or attached to each other.

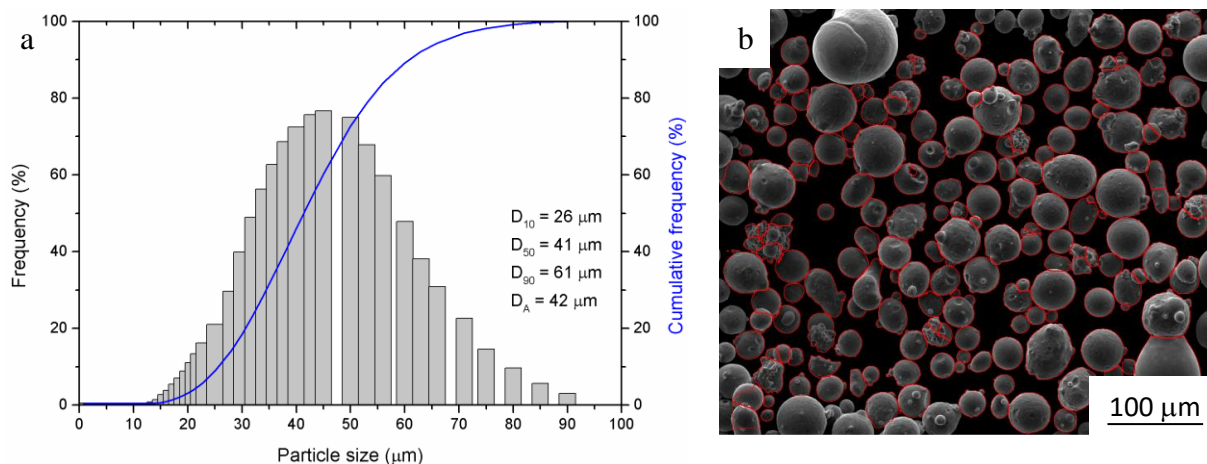


Figure 1: 15-5 PH particles: (a) result of laser diffraction particle size distribution; (b) morphological aspects. SEM – Secondary electrons image (SEI).

Density for EOS PH1 powder/as-built part is 7.8 g/cm^3 , which is close the actual measured of the powder, 7.76 g/cm^3 , and the one of the as-built, $7.63 \text{ g/cm}^3 (\pm 0.01 \text{ g/cm}^3)$, resulting in a relative density of the printed specimen of 98.3 % and the estimated porosity of 1.7%, which could also be performed by optical microscopy ⁽¹⁰⁾ and computed tomography ⁽⁹⁾. Other than on the fracture analysis, to be presented later, pores were hardly observed.

Very thin and random martensite laths (Fig. 2a - inset) compose most of the as-built sample. Also, as this is a cross-section to the building direction (BD), curved lines observed (red curved-interrupted lines) are molten pool boundaries (fish scale like), which are perpendicular to BD. While in the solution treated (and quenched to room temperature) sample (Fig. 2b), there are coarser martensite laths, when comparing to the as-built one. Random rips, about $20 \mu\text{m}$ long, are observed. No curved lines are present, making it a successful treatment. There is a circular pore ($\sim 5 \mu\text{m}$) by gas imprisonment (red arrow) in Fig. 2b.

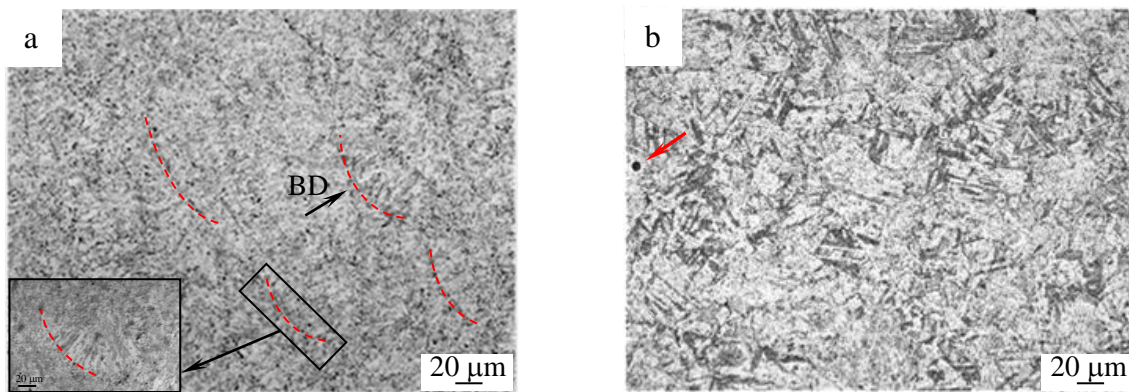


Figure 2: 15-5 PH Microstructure: (a) As-built (inset: martensite matrix); and (b) solution treated (and quenched to room temperature). Optical microscopy (OM) – Etchant: Villela’s (inset: 10ml HNO_3 , 10 ml acetic acid; 15 ml HCl ; and 3 drops of glycerin).

The as-built sample shows a dense array of dislocations (Fig. 3) in FIB-STEM images. Dislocations from geometrically necessary boundaries (GNBs) and incidental dislocation boundaries (IDBs)⁽⁶⁾ diffracted under bright field (BF) (Fig. 3a) and dark field (DF) (Fig. 3b), as expected in additive manufacturing owing to the severe thermal cycles and resulting tension. Precipitated phases of about 20 nm (arrow), also diffracted, but these are yet to be identified.

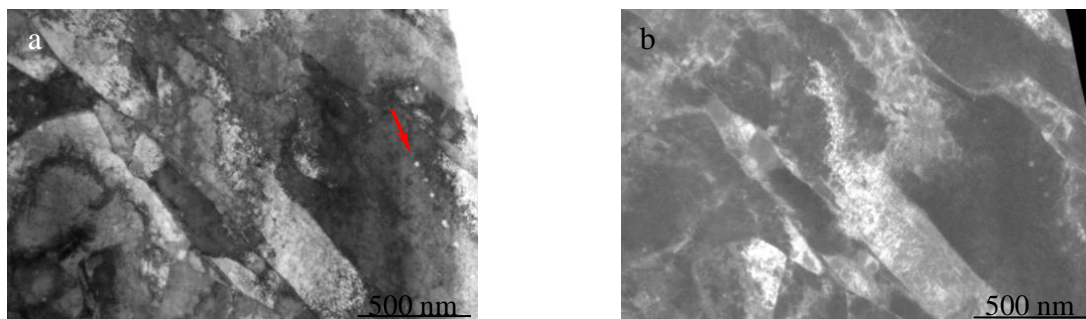


Figure 3: 15-5 PH as-built: (a) bright field; (b) dark field. FIB - STEM.

X-rays diffraction analysis (Fig. 4/ Table 3) shows martensite content dropping from 98.28 % to 97.37 %, as-built, so increasing the retained austenite content. Although the results reported by L.F. Kultz Unti et al ⁽³⁾ for retained austenite in an as-built sample is higher, one can speculate to be related to differences in processing, such as nitrogen ⁽¹¹⁾ pick up, that favors the M_f to lower temperatures.

The stress vs. strain curves (Fig. 5a) agree with the fracture SEM image analysis (Fig.5b) showing a highly ductile material with dimples developed, and few pores, notwithstanding the high resistance (Table 4). Hardness was measured in the Vicker's scale, average value of 415.2 HV (SD \pm 8.04).

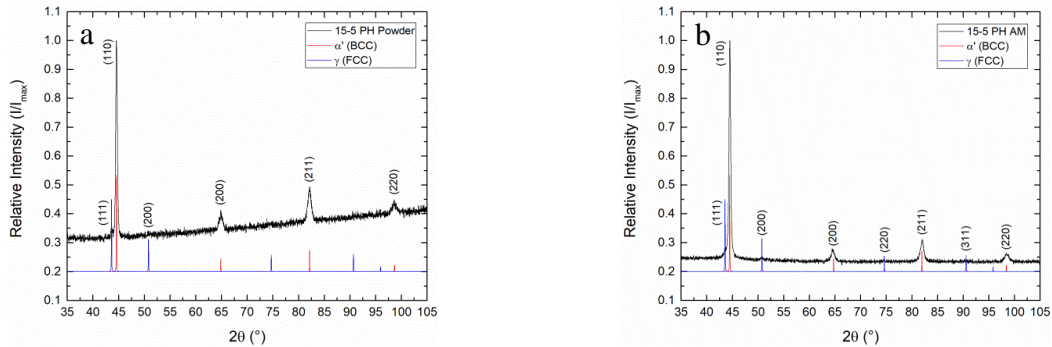


Figure 4: 15-5 PH X-rays diffraction patterns: (a) powder; and (b) as-built.

Table 3: 15-5 PH stainless steel: Results after Rietveld refinement.

Phase	α' (bcc)	γ (fcc)	α' (bcc)	γ (fcc)
	Powder		As-built	
Volume Fraction (%)	98.29	1.71	97.37	2.63
Lattice Constants a = b = c (nm)	0.28716	0.35924	0.28750	0.35959

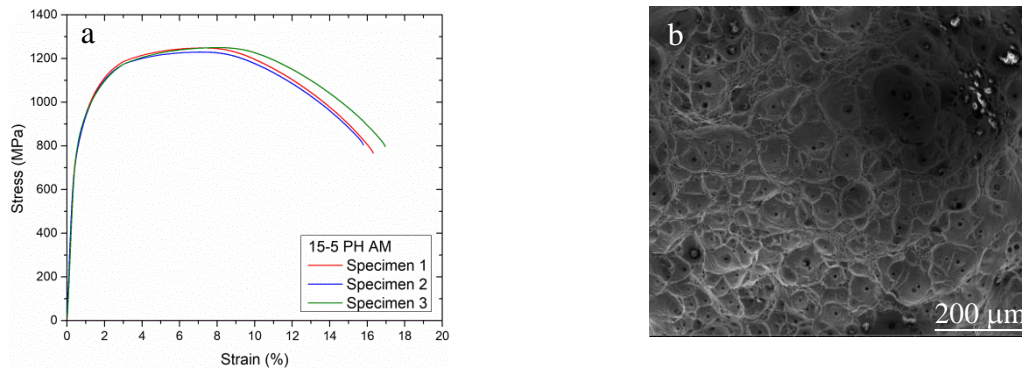


Figure 5: 15-5 PH: (a) Tensile testing, stress vs. strain curves; (b) ductile fracture surface – SEM, secondary electrons image (SEI).

Table 4: 15-5 PH additive as-built specimens: Mechanical properties - Tensile test results.

Properties		E (GPa)	YS (MPa)	TS (MPa)	EI (%)	AR (%)
As-built	Average	202.3	814.0	1,242.8	18.3	53.8
	St. Dev.	7.6	17.9	11.3	1.0	1.5

CONCLUSIONS

Considering AM using a 15-5 PH (EOS PH1) powder, a clear characterization path is disclosed from the metallic powder, where the whole process begins, to the as-built part. Actual density, measured from the powder, 7.76 g/cm³, and apparent, from as-built, 7.63 g/cm³, allowed estimating relative density of the specimen, 98.3 %, and porosity, 1.7%. The microstructure morphology evolved, from as-built to solution treated, from fine martensite to coarser one and the fish-scale, once in the as-built, disappeared in the solution treated sample. The as-built matrix presented high dislocation density and some precipitated

phases. Martensite is the major component in both the metallic powder and the as-built part, varying from 98.28 % to 97.37 %, and the second was retained austenite, 1.71 % to 2.63 %, both measures were made by X-rays diffraction.

Mechanical properties of the as-built specimens by tensile testing were $E = 202.3$ GPa, $YS = 814$ MPa, $UTS = 1,243.8$ MPa, and $EI = 18.3$ %, the fracture analysis showed very ductile features; and the average hardness measured was 415.2 HV.

ACKNOWLEDGEMENTS

The authors would like to thank CNPq for the financial support (postdoctoral research fellowships), and the National System of Nanotechnology Laboratories (MCTI/SisNANO/INT-CENANO-CNPq Process number 442604/2019-0). Also, to J. A. H. Medina to his collaboration and early discussions, to PUC/Rio's Departamento de Artes & Design, for 3D printing, and to LEBm/UFSC, for the chemical analysis of the as-built specimen.

REFERENCES

1. DEBROY, T. et al.. Additive manufacturing of metallic components – Process, structure and properties. *Progress in Materials Science*, v. 92, p. 112–224, mar. 2018.
2. ZHOU, T. et al.. Quantitative electron microscopy and physically based modelling of Cu precipitation in precipitation-hardening martensitic stainless steel 15-5 PH. *Materials and Design*, v. 143, p. 141–149, 2018.
3. KULTZ UNTI, L.F.; AOTA, L.S.; JARDINI, A.L.; et al.. Microstructural characterization of 15-5PH stainless steel processed by laser powder-bed fusion. *Materials Characterization*, New York, 2021. Available at: < <https://doi.org/10.1016/j.matchar.2021.111485> > DOI: 10.1016/j.matchar.2021.111485.
4. COUTURIER, L. et al.. Evolution of the microstructure of a 15-5PH martensitic stainless steel during precipitation hardening heat treatment. *Materials and Design*, v. 107, p. 416–425, 2016.
5. HABIBI BAJGUIRANI, H. R.. Mechanism of austenitic transformation in the martensitic stainless steel of type PH 15-5. *Journal de Physique IV*, v. 4, p. C3-123-C3-126, 1994.
6. HUGHES, D.; BAMMANN, D.. Geometrically necessary boundaries, incidental dislocation boundaries and geometrically necessary dislocations. v. 25, p. 147-153, 2003.
7. COUTURIER, L.. Caractérisation des évolutions microstructurales de l'acier inoxydable martensitique à durcissement structural 15-5PH au cours du vieillissement thermique. 2014. 201p. Thesis (l'École Doctorale Ingénierie - Matériaux Mécanique Énergétique Environnement Procédés Production (I-MEP2)) - Université de Grenoble, Grenoble.
8. ŠIŠAK JUNG, D.; et al. High-energy X-ray applications: current status and new opportunities. *Powder Diffraction*, v. 32, n. S2, p. 2–7, 2017.
9. KHOSRAVANI, M. R.; REINICKE, T.. On the use of X-ray computed tomography in assessment of 3D-printed components. *Journal of Nondestructive Evaluation*, v. 39 (75), p.1-17, 2020. <https://doi.org/10.1007/s10921-020-00721-1>.
10. KHAIRALLAH, S. A.; et al.. Laser powder-bed fusion additive manufacturing: Physics of complex melt flow and formation mechanisms of pores, spatter, and denudation zones. *Acta Materialia*, v. 108, p. 36–45, 2016.
11. MURR, L. E.; MARTINEZ, E.; HERNANDEZ, J.; COLLINS, S.; AMATO, K. N.; GAYTAN, S. M.; SHINDO, P. W.. Microstructures and properties of 17-4 PH stainless steel fabricated by selective laser melting. *Journal of Materials Research and Technology*, v. 1 (3), p. 167-177, 2012.